Systematic investigation of projectile fragmentation using beams of unstable B and C isotopes

R. Thies,[1,*] A. Heinz,[1] T. Adachi,[2] Y. Aksyutina,[3,4] J. Alcantara-Núñes,[5] S. Altstadt,[6] H. Alvarez-Pol,[5] N. Ashwood,[7] T. Aumann,[3,4] V. Avdeichikov,[8] M. Barr,[7] S. Beceiro-Novo,[9] D. Bemmerer,[10] J. Benlliure,[5] C. A. Bertulani,[11] K. Boretzky,[4] M. J. G. Borge,[12] G. Burgunder,[13] M. Camaño,[5] C. Caesar,[3,4] E. Casarejos,[14] W. Catford,[15] J. Cederkäll,[8] S. Chakraborty,[16] M. Chartier,[17] L. V. Chulkov,[4,18] D. Cortina-Gil,[5] R. Crespo,[19] U. Datta,[16] P. Díaz Fernández,[5] I. Dillmann,[4,20] Z. Elekes,[21] J. Enders,[3] O. Ershova,[6] A. Estradé,[4,22] F. Farinon,[4] L. M. Fraile,[23] M. Freer,[7] M. Freudenberger,[3] H. O. U. Fynbo,[24] D. Galaviz,[25] H. Geissel,[4,20] R. Gernhäuser,[26] K. Göbel,[6] P. Golubev,[8] D. Gonzalez Diaz,[3] J. Hagdahl,[1] T. Heftrich,[6] M. Heil,[4] M. Heine,[3] A. Henriques,[25] M. Holl,[3] G. Ickert,[4] A. Ignatov,[3] B. Jakobsson,[8] H. T. Johansson,[1] B. Jonson,[1] N. Kalantar-Nayestanaki,[2] R. Kanungo,[22] R. Knöbel,[4,20] T. Kröll,[3] R. Krücken,[26] J. Kurcewicz,[4] N. Kurz,[4] M. Labiche,[27] C. Langer,[6] T. Le Bleis,[26] R. Lemmon,[27] O. Lepyoshkina,[26] S. Lindberg,[1] J. Machado,[25] J. Marganiec,[3,28] V. Maroussov,[29] M. Mostazo,[5] A. Movsesyan,[3] A. Najafi,[2] T. Nilsson,[1] C. Nociforo,[4] V. Panin,[3] S. Paschalis,[3] A. Perea,[12] M. Petri,[3] S. Pietri,[4] R. Plag,[6] A. Prochazka,[4] A. Rahaman,[16] G. Rastrepina,[4] R. Reifarth,[6] G. Ribeiro,[12] M. V. Ricciardi,[4] C. Rigollet,[2] K. Riisager,[24] M. Röder,[10,30] D. Rossi,[4] J. Sanchez del Rio,[12] D. Savran,[4,28] H. Scheit,[3] H. Simon,[4] O. Sorlin,[13] V. Stoica,[2,31] B. Streicher,[2,4] J. T. Taylor,[17] O. Tengblad,[12] S. Terashima,[4] Y. Togano,[28] E. Uberseder,[32] J. Van de Walle,[2] P. Velho,[25] V. Volkov,[3,18] A. Wagner,[10] F. Wamers,[3,4] H. Weick,[4] M. Weigand,[6] C. Wheldon,[7] G. Wilson,[15] C. Wimmer,[6] J. S. Winfield,[4] P. Woods,[33] D. Yakorev,[10] M. V. Zhukov,[1] A. Zilges,[29] and K. Zuber[30]

(R3B Collaboration)

[1]*Institutionen för Fysik, Chalmers Tekniska Högskola, 412 96 Göteborg, Sweden*

[2]*KVI-CART, University of Groningen, Zernikelaan 25, 9747 AA Groningen, The Netherlands*

[3]*Institut für Kernphysik, Technische Universität Darmstadt, 64289 Darmstadt, Germany*

[4]*GSI Helmholtzzentrum für Schwerionenforschung, 64291 Darmstadt, Germany*

[5]*Dpt. de Física de Partículas, Universidade de Santiago de Compostela, 15706 Santiago de Compostela, Spain*

[6]*Goethe-Universität Frankfurt am Main, 60438 Frankfurt am Main, Germany*

[7]*School of Physics and Astronomy, University of Birmingham, Birmingham B15 2TT, United Kingdom*

[8]*Department of Physics, Lund University, 22100 Lund, Sweden*

[9]*National Superconducting Cyclotron Laboratory, Michigan State University, East Lansing, Michigan 48824, USA*

[10]*Helmholtz-Zentrum Dresden-Rossendorf, 01328 Dresden, Germany*

[11]*Department of Physics and Astronomy, Texas A&M University-Commerce, Commerce, Texas 75429, USA*

[12]*Instituto de Estructura de la Materia, CSIC, Serrano 113 bis, 28006 Madrid, Spain*

[13]*GANIL, CEA/DSM-CNRS/IN2P3, B.P. 55027, 14076 Caen Cedex 5, France*

[14]*University of Vigo, 36310 Vigo, Spain*

[15]*Department of Physics, University of Surrey, Guildford GU2 7XH, United Kingdom*

[16]*Saha Institute of Nuclear Physics, 1/AF Bidhan Nagar, Kolkata-700064, India*

[17]*Oliver Lodge Laboratory, University of Liverpool, Liverpool L69 7ZE, United Kingdom*

[18]*Kurchatov Institute, 123182 Moscow, Russia*

[19]*Instituto Superior Técnico, University of Lisbon, Lisboa, 1049-001 Lisboa, Portugal*

[20]*II. Physikalisches Institut, Universität Gießen, 35392 Gießen, Germany*

[21]*MTA Atomki, 4001 Debrecen, Hungary*

[22]*Astronomy and Physics Department, Saint Mary's University, Halifax, NS B3H 3C3, Canada*

[23]*Facultad de Ciencias Físicas, Universidad Complutense de Madrid, Avda. Complutense, 28040 Madrid, Spain*

[24]*Department of Physics and Astronomy, Aarhus University, 8000 Århus C, Denmark*

[25]*Centro de Fisica Nuclear, University of Lisbon, 1649-003 Lisbon, Portugal*

[26]*Physik Department E12, Technische Universität München, 85748 Garching, Germany*

[27]*STFC Daresbury Laboratory, Daresbury, Warrington WA4 4AD, United Kingdom*

[28]*ExtreMe Matter Institute, GSI Helmholtzzentrum für Schwerionenforschung GmbH, 64291 Darmstadt, Germany*

[29]*Institut für Kernphysik, Universität zu Köln, 50937 Köln, Germany*

[30]*Institut für Kern- und Teilchenphysik, Technische Universität Dresden, 01069 Dresden, Germany*

[31]*Department of Sociology / ICS, University of Groningen, 9712 TG Groningen, The Netherlands*

[32]*Department of Physics, University of Notre Dame, Notre Dame, Indiana 46556, USA*

[33]*School of Physics and Astronomy, University of Edinburgh, Edinburgh EH9 3JZ, United Kingdom*

(Received 2 March 2016; published 2 May 2016)

Background: Models describing nuclear fragmentation and fragmentation fission deliver important input for planning nuclear physics experiments and future radioactive ion beam facilities. These models are usually benchmarked against data from stable beam experiments. In the future, two-step fragmentation reactions with

*ronja.thies@chalmers.se

exotic nuclei as stepping stones are a promising tool for reaching the most neutron-rich nuclei, creating a need for models to describe also these reactions.

Purpose: We want to extend the presently available data on fragmentation reactions towards the light exotic region on the nuclear chart. Furthermore, we want to improve the understanding of projectile fragmentation especially for unstable isotopes.

Method: We have measured projectile fragments from $^{10,12-18}$C and $^{10-15}$B isotopes colliding with a carbon target. These measurements were all performed within one experiment, which gives rise to a very consistent data set. We compare our data to model calculations.

Results: One-proton removal cross sections with different final neutron numbers ($1pxn$) for relativistic $^{10,12-18}$C and $^{10-15}$B isotopes impinging on a carbon target. Comparing model calculations to the data, we find that the EPAX code is not able to describe the data satisfactorily. Using ABRABLA07 on the other hand, we find that the average excitation energy per abraded nucleon needs to be decreased from 27 MeV to 8.1 MeV. With that decrease ABRABLA07 describes the data surprisingly well.

Conclusions: Extending the available data towards light unstable nuclei with a consistent set of new data has allowed a systematic investigation of the role of the excitation energy induced in projectile fragmentation. Most striking is the apparent mass dependence of the average excitation energy per abraded nucleon. Nevertheless, this parameter, which has been related to final-state interactions, requires further study.

DOI: 10.1103/PhysRevC.93.054601

I. INTRODUCTION

Since the advent of radioactive ion beam facilities it has been possible to study more exotic isotopes, which has led to new discoveries, like halo nuclei and the changing of magic numbers with isospin. For a recent overview see, e.g., Refs. [1,2]. Reaction cross sections involving exotic nuclei allow us to extract nearly model-independent observables, in contrast to other reaction processes, such as nucleon transfer, which are strongly dependent on the reaction mechanism adopted for the experimental analysis. Indeed, reaction cross sections have led to a number of interesting discoveries such as the above-mentioned halo nuclei [3].

Models describing nuclear fragmentation and fragmentation fission deliver important input to yield predictions useful for planning of experiments and future accelerator facilities [4]. Recently, two-step fragmentation reactions have been discussed for future facilities [5] and are already used [6] to reach especially neutron-rich nuclei.

There exist several models for the prediction of reaction cross sections, examples are models following the abrasion-ablation, the intranuclear cascade approach, and empirical parametrizations. As the models are usually benchmarked with stable nuclei – while exotic nuclei can exhibit different behavior – their ability to predict fragmentation cross sections for exotic nuclei is unclear. We investigate whether fragmentation models are able to describe reaction cross sections of light exotic nuclei, which exhibit such a rich variety of properties.

We have systematically measured one-proton–x-neutron ($1pxn$) removal cross sections for $0 \leqslant x \leqslant 5$ for a large range of carbon and boron isotopes impinging on carbon targets at relativistic energies. We compare our measured $1pxn$ removal cross sections to calculations of an abrasion-ablation model (ABRABLA07 [7]). We also compare them to the widely used EPAX code [8] though it is limited to $A > 40$, since it has been used earlier for lighter nuclei. Leistenschneider *et al.* [9] performed a similar study for the less exotic $^{17-21}$O isotopes, comparing both models to their data. The comparison was unsatisfactory, but subsequently both models have been improved.

II. EXPERIMENT

The experiment was conducted using the LAND/R^{3}B setup at the GSI Helmholtz Centre for Heavy Ion Research in Germany, and was designed as an overview experiment covering isotopes with $Z = 3$ to $Z = 9$ between the extremes of isospin. The radioactive beams were produced from an ^{40}Ar primary beam at 490A MeV[1] impinging on a 4 g/cm^2 Be target. To separate and select the secondary beams the projectile fragment separator (FRS) [10] was used. With five different separator settings, beams with (centered) A/Z ratios ranging from 1.66 to 3 were selected and guided to the experimental setup. The secondary beams had kinetic energies in the range of $390A - 430A$ MeV. Reaction targets of C (0.56 and 0.93 g cm^{-2}) as well as an empty target frame were used in this work.

The LAND/R^{3}B setup, shown in Fig. 1, is designed for complete kinematics measurements on an event-by-event basis. At relativistic beam energies, the setup benefits from kinematic forward focusing of the reaction products, resulting in almost full acceptance in the center-of-mass frame. The incoming ions are characterized by their magnetic rigidity (defined by the FRS), by their time of flight (TOF) between the FRS and the setup measured by plastic scintillator detectors (POS), and by energy-loss measurements (ΔE) in a silicon PIN diode (PSP) upstream from the reaction target. Located directly in front of and behind the reaction target are pairs of double-sided-silicon-strip detectors, SST1 through SST4 (100 μm pitch), determining the angle and charge of incoming and outgoing ions.

Light reaction products emitted at laboratory angles $>7.5^\circ$ are detected in the segmented NaI array Crystal Ball (XB)

[1]Here, and in all further uses of the unit A MeV, we neglect the binding energy.

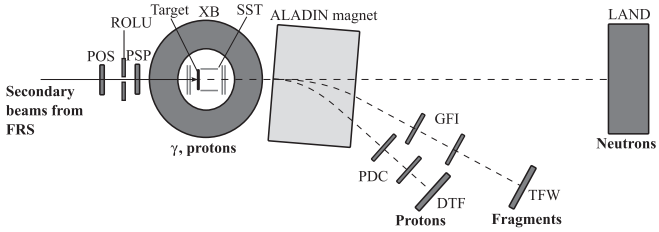

FIG. 1. Schematic view of the LAND/R^{3}B setup seen from above. The most important detectors for this work are POS, ROLU, PSP, SST, GFI, TFW, and XB. POS provides energy-loss (ΔE) and time-of-flight (TOF) measurements. ROLU is an active veto detector on the incoming beam. PSP and SST are used for ΔE measurements, the main purpose of the SST is to determine incoming and outgoing directions of the beam. The GFIs provide tracking of the beam behind the magnet ALADIN, and the TFW provides TOF, ΔE, and position information. The XB is a calorimeter for protons and γs, and is here solely used for trigger purposes. For a more detailed description of the setup see text. This schematic is not to scale.

[11] surrounding the target. By means of a dual readout in the forward direction [12] (up to 63° from the beam direction) the array is capable of detecting both photons and protons emitted at large angles, though with limited angular precision (≈77 msr solid angle per segment).

Charged fragments are bent by the dipole magnet ALADIN and subsequently detected in fibre detectors (GFIs) [13] for position determination in the bending plane. After a total flight path of around 10 m behind the target, the fragments are detected in a plastic TOF wall (TFW) providing time, energy loss, and coarse position information.

Beam-like protons emitted at small angles (<7.5°) also traverse the magnet and are detected by two drift chambers (PDCs) and a TOF wall (DTF). Neutrons (emitted at angles <7.5°) are detected in the forward direction, about 12 m downstream from the target in the neutron detector LAND [14]. The data presented in this work do not require reconstruction of neutrons and light reaction products. Though the setup also allows detailed spectroscopic analysis, this is not within the scope of this work. Cross-section measurements require significantly less statistics, and therefore allow an overview of all ions in the experiment (we restrict ourselves here to boron and carbon).

III. ANALYSIS

The incoming beam is selected[2] by fitting the charge versus mass-to-charge-ratio distribution [see Fig. 2(a)] with two-dimensional (2D) Gaussian distributions. Only ions inside the 2σ selection around the mean value, extracted from the fit, are taken into account in the analysis. To further reduce misidentifications arising from pile-up, a second additional charge identification using ΔE measurements from POS and the SST detector just upstream from the target is employed, following the same pattern: fitting of 2D Gaussian distributions and selecting ions inside 2σ from the mean.

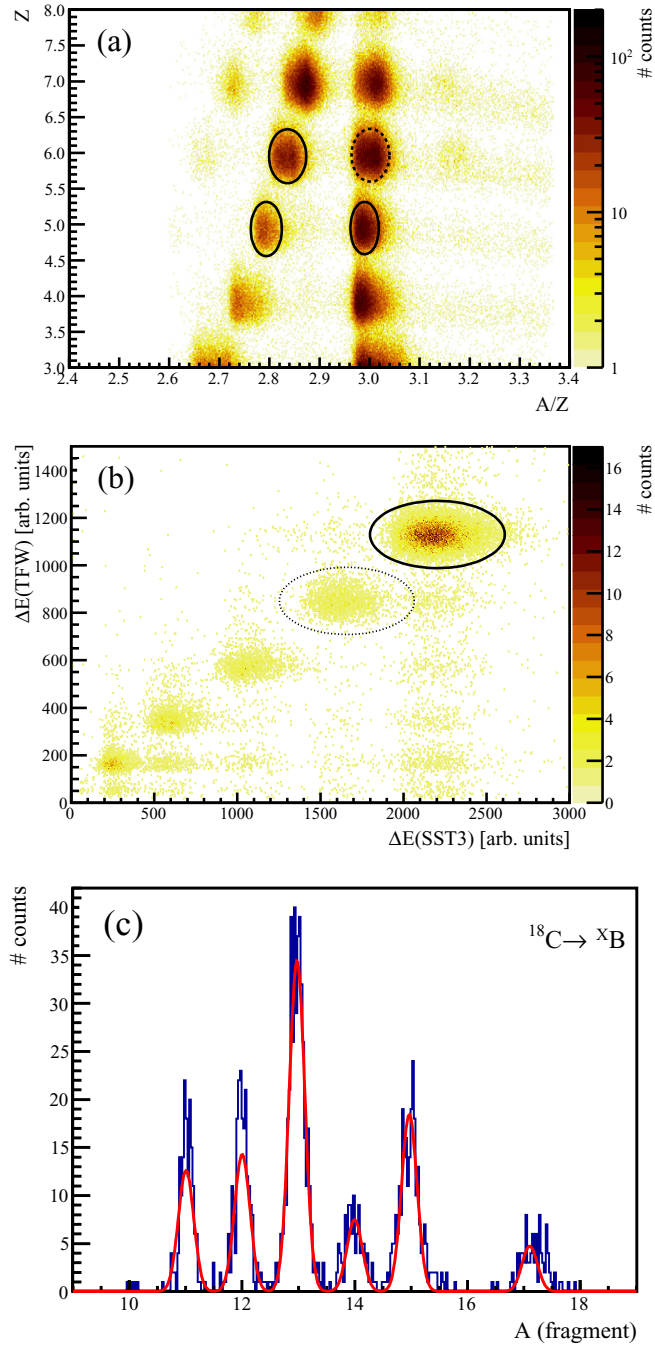

FIG. 2. Illustration of the reaction identification (ID). (a) Shows the incoming ID with charge versus mass-to-charge ratio. The ellipses indicate the 2σ selection of different isotopes. The dashed ellipse represents the selection used for the data in plots (b) and (c). (b) Presents the charge identification after the reaction target, using ΔE measurements at the end of the setup versus in the first detector behind the reaction target. The ellipses indicate the 3σ selection of the unreacted beam (solid) and 1pxn reaction (dotted). (c) Shows the reconstructed mass from the 1pxn removal and the fit to the spectrum. For details see text.

[2]To ensure reproducibility: for calibration and unpacking the LAND02 software package with the following git-tags was used: ronja-r3bm-5-2015 (LAND02) and ronja-6-2015 (calibration parameters).

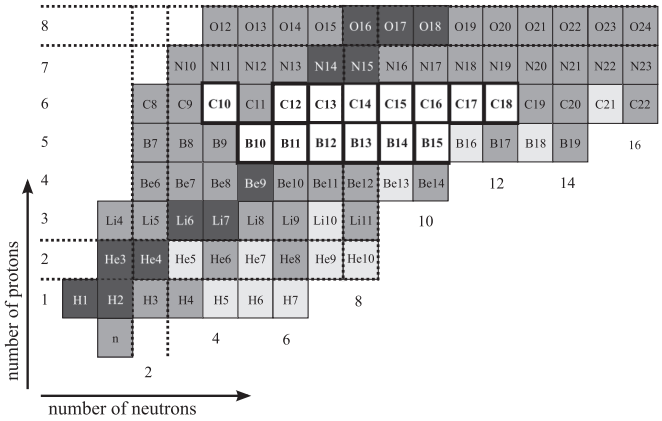

FIG. 3. Excerpt from the nuclear chart, illustrating the isotopes selected from the incoming secondary beams (white, thick frame). All carbon and boron isotopes with sufficient statistics were used.

The charge of the outgoing ion is identified by using ΔE measurements in the SST detector directly downstream from the target (SST3) and the TOF detector at the end of the setup (TFW), thus ensuring that no charge-changing reactions take place while the fragment travels through the setup behind the target, see Fig. 2(b). The same technique of 2D-Gaussian distribution fits, but now with a 3σ selection is used.

The mass of the outgoing fragment is calculated using the map of the magnetic field of ALADIN, the direction of the ion after the target, the direction after the magnet, and the time of flight through the setup using χ^2 minimization of a Runge-Kutta propagation[3] [15] of the ion through the setup. An example of the resulting mass distribution for a $1pxn$ removal reaction is presented in Fig. 2(c). We employ a fit of a sum of Gaussian distributions (where the number of distributions in the sum corresponds to the number of different isotopes produced) to these mass distributions, and extract the number of outgoing ions of a certain isotope using the fit parameters. Isotopes with cross sections below $\approx$2 mb do not have sufficient statistics, thus no cross sections are reported. Due to acceptance limits, no cross sections for neutron-loss channels with more than five neutrons ($\Delta N > 5$) could be extracted.

The cross sections are normalized using the unreacted beam, which is identified and reconstructed in the same way as the reacted beam. Together with the $\Delta N \leqslant 5$ condition, ensuring that the fragment is inside the acceptance of our setup, this renders efficiency corrections for beam detectors unnecessary.

Two different trigger patterns[4] are used in this analysis. For selection of the unreacted beam, the "fragment trigger" which requires valid TOF signals and no veto of the incoming beam (cf. Fig. 1, ROLU), is used. For the reacted beam a "XB-reaction trigger" was used, requiring in addition to the same conditions as the fragment trigger, also the detection of an energy signal in the calorimeter surrounding the target (XB). The calorimeter detects γ rays and light particles at angles $\geqslant 7.5^\circ$ with respect to the beam axis. An energy signal in the XB indicates therefore that a reaction took place. The trigger efficiency of the XB-reaction trigger is experimentally determined to be $(85.3 \pm 2.5)\%$ of the trigger efficiency of the fragment trigger.

The reaction probability of the carbon and boron isotopes in the carbon targets is $(0.9 \pm 0.2)\%$ and $(0.8 \pm 0.2)\%$ for the thinner and $(1.5 \pm 0.3)\%$ and $(1.3 \pm 0.3)\%$ for the thicker targets, respectively. The probability of multiple reactions in the target is thus insignificant.

IV. RESULTS

We have extracted one-proton–x-neutron ($1pxn$) removal cross sections for $0 \leqslant x \leqslant 5$ for beams of carbon isotopes of mass 10 and 12–18, and boron isotopes of mass 10–15 on a C target. The location of these isotopes on the nuclear chart is illustrated in Fig. 3. Several isotopes were present in

TABLE I. Summary of the extracted $1pxn$ removal cross sections. The error provided represents the statistical uncertainty. The systematic uncertainty due to uncertainties in the target thickness and trigger efficiency is estimated to be 5%.

A_{in}	Z_{in}	A_{out}	σ (mb)	Error (mb)	A_{in}	Z_{in}	A_{out}	σ (mb)	Error (mb)
18	6	17	10.2	1.4	15	5	14	4.0	1.0
18	6	15	39.9	3.2	15	5	12	31.7	2.5
18	6	14	16.2	1.8	15	5	11	29.1	2.7
18	6	13	74.7	5.3	15	5	10	65.5	5.5
18	6	12	30.9	3.0	15	5	9	10.8	1.7
17	6	15	27.9	1.8	14	5	12	21.3	1.2
17	6	14	14.1	1.2	14	5	11	20.6	1.2
17	6	13	72.5	3.7	14	5	10	62.8	2.9
17	6	12	40.9	2.6	14	5	9	13.2	1.0
17	6	11	40.2	2.5					
16	6	15	20.5	0.4	13	5	12	8.9	0.3
16	6	14	11.9	0.3	13	5	11	19.8	0.5
16	6	13	65.3	1.0	13	5	10	58.4	1.1
16	6	12	43.0	0.7	13	5	9	17.6	0.5
16	6	11	53.7	0.9					
16	6	10	4.1	0.2					
15	6	14	27.3	1.2	12	5	11	6.8	0.3
15	6	13	40.9	1.6	12	5	10	59.3	1.6
15	6	12	47.3	1.8	12	5	9	20.6	0.7
15	6	11	67.7	2.6	12	5	7	3.5	0.2
15	6	10	10.4	0.7					
14	6	13	51.1	1.4	11	5	10	37.0	1.3
14	6	12	34.6	1.1	11	5	9	19.9	0.8
14	6	11	84.8	2.2	11	5	7	3.0	0.3
14	6	10	16.7	0.7					
13	6	12	55.5	1.3	10	5	9	13.3	1.6
13	6	11	76.2	1.8	10	5	7	10.6	1.6
13	6	10	26.8	0.9					
12	6	11	85.4	3.1					
12	6	10	48.8	2.2					
10	6	8	13.3	3.0					

[3]To ensure reproducibility: LAND/R^{3}B TRACKER software was used with the git-tag ronja-r3bm-5-2015.

[4]A trigger pattern is a certain combination of detectors firing, it is used for selecting which events are recorded.

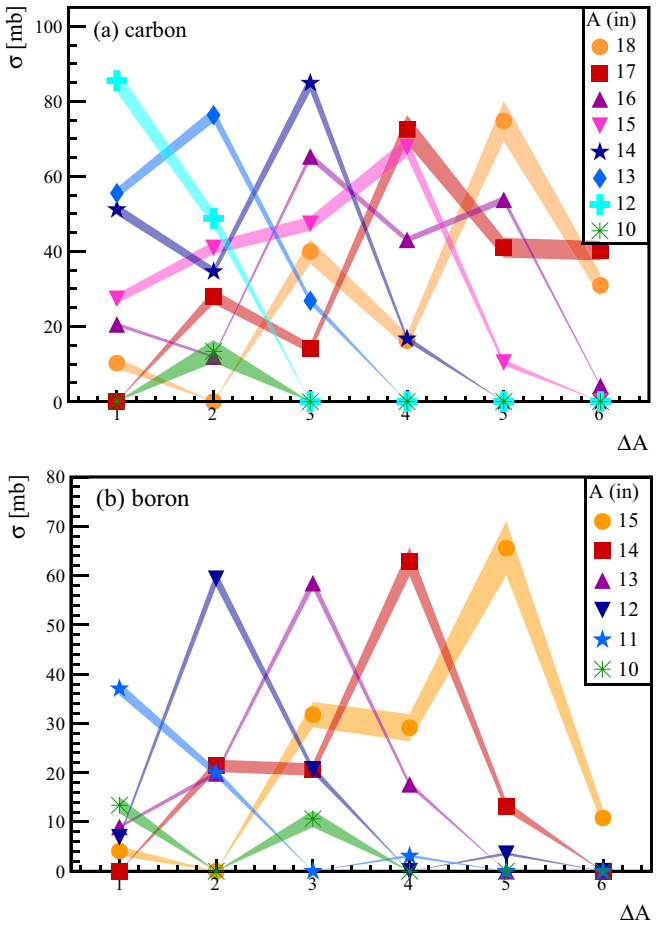

FIG. 4. $1pxn$ removal cross sections plotted versus the change in nucleon number for carbon and boron. The shaded area represents the statistical error bar. For boron there is a strong trend that the cross section for populating the long-lived ^{10}Be is largest for all incoming isotopes. For carbon isotopes the cross section to produce the heaviest available stable isotope, ^{11}B is largest, except for very neutron-rich isotopes, where instead the cross section to the semimagic ^{13}B becomes largest, with the transition point located at ^{16}C.

more than one fragment separator setting, and had therefore slightly different kinetic energies (390A to 430A MeV). The cross sections at the slightly different energies, as expected [16], did not show any energy dependence in this interval and were averaged with respect to their statistical weights. The averaged cross sections are provided in Table I and shown in Fig. 4, which presents the production cross section versus ΔA (difference in number of nucleons between mother and daughter nuclei) for incoming carbon and boron isotopes. For the latter we observe a strong trend in the production cross section of ^{10}Be. It is the largest of all measured $1pxn$ cross sections for all isotopes for which the $1pxn$ removal leaves a Be isotope with mass 10 or larger. For the carbon isotopes the trend is not as clear. Carbon isotopes lighter than mass 16 show clearly the largest $1pxn$ cross section for ^{11}B, while those heavier than mass 15 have the largest cross section for semimagic ^{13}B. The transition point is ^{16}C, featuring large production cross sections for both ^{11}B and ^{13}B. A separate case is ^{10}C which is proton rich and for which only the $1p1n$ reaction populates a bound nucleus (^{8}B).

V. MODEL CALCULATIONS

The model we use to understand the physics connected to our data is ABRABLA07 [7], which is a standard code for the description of fragmentation and fragmentation-fission reactions of heavy nuclei. It describes these reactions quite successfully (see, e.g., Ref. [17]). Fragmentation is described by the model as a two-step process – abrasion and ablation – the former determining how many nucleons are removed in the collision, and the latter which and how many light particles are evaporated owing to the excitation energy induced by the collision. Both parts use the Monte Carlo approach.

The abrasion part uses Karol's approximation [18] to extract the total interaction cross section. The number of removed nucleons is calculated from the geometrical overlap of the colliding nuclei, based on the impact parameter; while the neutron-proton ratio of the prefragment is calculated from the hyper-geometrical distribution [7]. The excitation energy of the daughter nucleus is determined from the single-particle energies of the removed nucleons, which is on average 13.5 MeV per abraded nucleon [7]. It was found [19] that the excitation energy has to be multiplied by a factor of 2 in order to reproduce experimental data, which is motivated by the final-state interactions of participants and spectators.

The ablation part, described in detail in Ref. [20], bases the particle emission on the statistical model and the Weisskopf-Ewing formalism [21]. Level densities are calculated using the Fermi-gas approach [22], modulated by nuclear structure

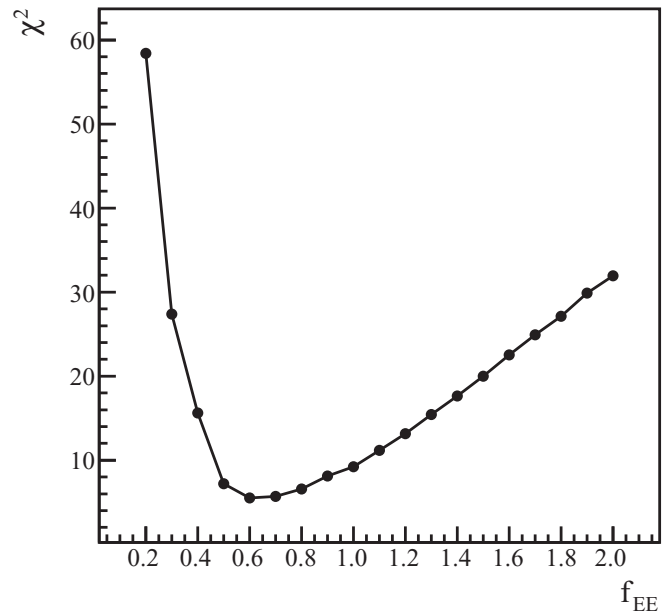

FIG. 5. χ^2 versus the excitation energy multiplication factor used in the ABRABLA07 [7] calculations. χ^2 is determined as described in the text, summed for all experimentally determined cross sections measured in this work. Lines are used to guide the eye.

effects (e.g., collective enhancement), which at low excitation energies is replaced by the constant-temperature model [23].

Calculations were performed running 10^6 collisions per incoming ion, rendering the statistical uncertainty of the calculated cross sections of 3 mb (the smallest experimental data point) to be below 2%.

VI. DISCUSSION

To optimize the input parameters of ABRABLA07, we used the mass evaluation from 2012 [24,25] instead of the mass evaluation from 2003 and added a few missing unbound nuclei. Both modifications resulted in very minor changes of the cross sections.

To be able to reproduce the cross sections of the light nuclei measured in this work, we had to decrease the multiplication factor of the excitation energy to 0.6. This was deduced from a systematic study of the ability of ABRABLA07 to reproduce the experimental cross sections depending on the excitation energy multiplication factor f_{EE}. The study was performed by running ABRABLA07 calculations with an f_{EE} varying between 0.2 and 2, in steps of 0.1. Using both the statistical and known

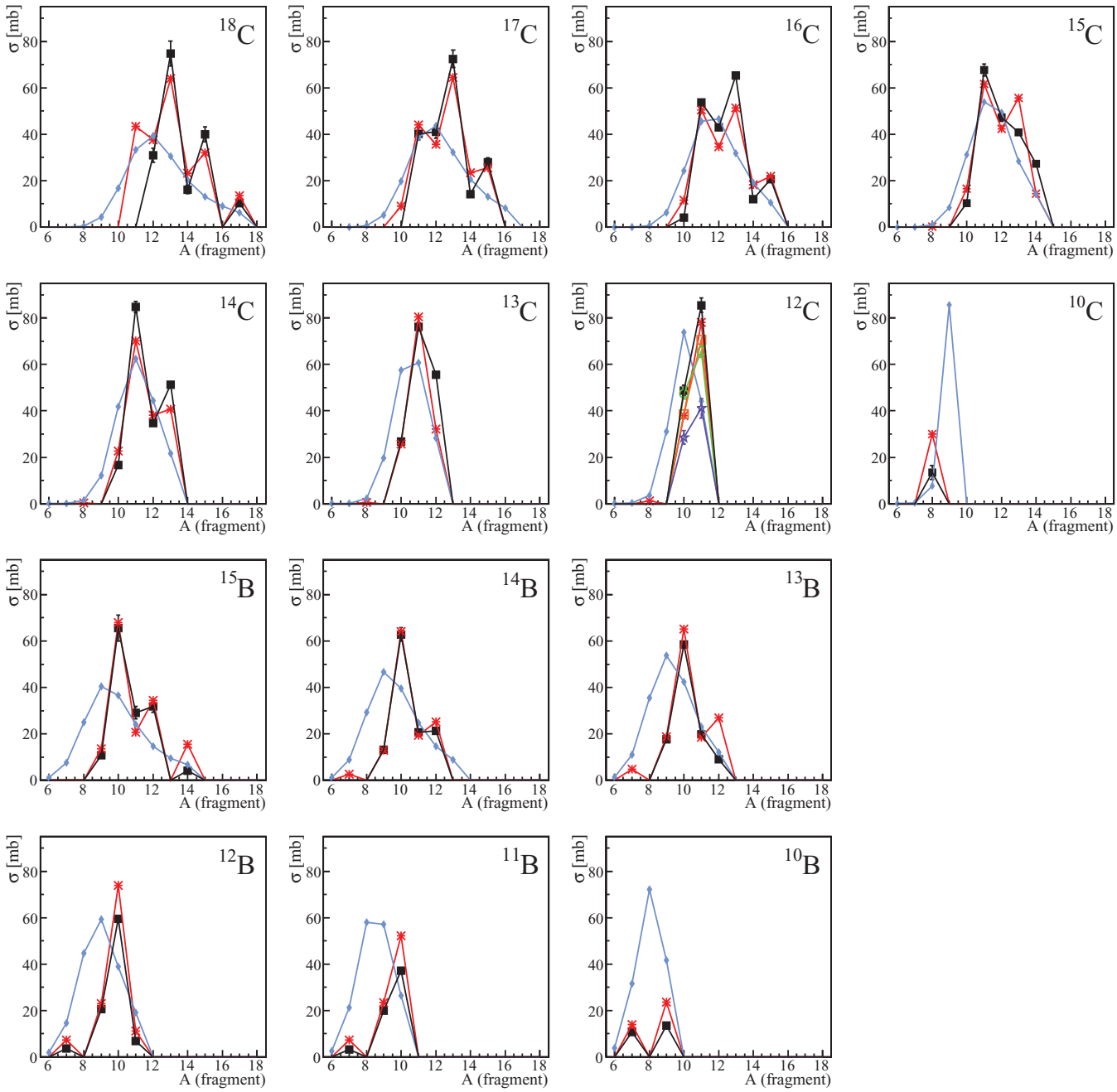

FIG. 6. Comparison between ABRABLA07 [7] (red stars), EPAX [4,28] (blue diamonds), and the experimental data (black full squares). For ^{12}C experimental data from three other measurements of ^{12}C on C are shown: at 600A MeV, Ref. [26] (orange empty square,); at 250A MeV, Ref. [27] (green empty circles); and at 400A MeV, Ref. [16] (purple bold stars).

systematic uncertainty we calculated a χ^2 for the agreement between calculation and data for each incoming isotope and f_{EE}. The result of the total χ^2 per isotope, which is the sum of the individual χ^2 of all incoming isotopes divided by the amount of daughter isotopes, is illustrated in Fig. 5. The minimum is located at 0.6, indicating that all isotopes simultaneously are best described by an f_{EE} of 0.6, i.e., an average excitation energy of 8.1 MeV per abraded nucleon.

The complete comparison of the calculations with the best fit f_{EE} (= 0.6) with the data is shown in Fig. 6. First, one should note that our experimental data for stable ^{12}C agrees with data from previous stable beam experiments [26,27]. Data taken by Ogawa *et al.* [16] disagrees somewhat with both our and the other previous measurements.

Altogether, ABRABLA07, which is designed for calculation of fragmentation and fission cross sections of heavier nuclei and employs several approximations based on the properties of these, reproduces the data very well. We still observe a few differences between model and data. Generally the prediction for $1pxn$ removal cross sections for B is much better than the prediction for $1pxn$ removal from C. The $1p0n$ channels are generally overestimated for boron by ABRABLA07. For carbon no such trend is visible.

Another widely used model is EPAX developed by Sümmerer [8], which we also show for comparison (in Fig. 6). Our data are outside the range limit of EPAX, which is $A > 40$, but EPAX has previously been used for lower masses (e.g., in Ref. [9]). This empirical formula misses details of the structure in this region of the nuclear chart and has therefore only limited applicability for such light nuclei.

A best fit $f_{\mathrm{EE}} = 0.6$ for our data is quite different from the originally published f_{EE} of 2.0 from peripheral collisions of the much heavier ^{197}Au [19]. The final-state interactions, proposed as physics motivation for introducing the f_{EE}, should, from naive geometry arguments, scale with the size of the nuclei. To further understand the influence of the excitation energy multiplication factor on the ability of ABRABLA07 to reproduce the $1pxn$ cross sections, we investigate the dependence of f_{EE} on the projectile mass. To do that we use data from Refs. [6,26,29–34], as summarized in Table II, and perform ABRABLA07 calculations with f_{EE} between 0.5 and 4 in intervals of 0.1. With the requirements of beam energies above 100A MeV and data available in tabulated form, we used all to our knowledge published $1pxn$ removal data available.

For heavier isotopes, in contrast to light isotopes, the possibility of very long evaporation chains exists. These long evaporation chains are caused by reactions in which more excitation energy is generated in the abrasion step which corresponds to more violent, nonperipheral collisions. In order to compare similar collisions, we restrict ourselves to a maximum of five removed neutrons in this analysis, which corresponds to the same range as in our light nuclei. We calculate the χ^2 (for each f_{EE} and isotope), as above, which is then used to determine the best f_{EE} for each isotope. For some isotopes no minimum could be found. This stems from a too large mismatch of the cross sections in our area of interest. The error is estimated by looking at which f_{EE}, other than the best, have a χ^2 smaller than the best $\chi^2 + 1\sigma_{\chi^2}$. The error of the χ^2 is estimated by standard error propagation. The largest possible difference between the f_{EE} still having $\chi^2 \leqslant \chi^2_{\mathrm{best}} + 1\sigma_{\chi^2,\mathrm{best}}$ is determined for f_{EE} being both smaller and larger than the best f_{EE} and their average gives the estimated uncertainty. Large errors are caused by a mismatch between data and calculation concerning the trend of cross section vs removed neutrons.

TABLE II. Isotopes used to study the mass dependence of the f_{EE}, sorted by publication. For isotopes marked with an asterisk no minimal χ^2 and therefore no optimal f_{EE} could be determined.

Reference	Isotope
This work	^{10}B, ^{10}C, ^{11}B, ^{12}B, ^{12}C, ^{13}B, ^{13}C, ^{14}B, ^{14}C, ^{15}B, ^{15}C, ^{16}C, ^{17}C, ^{18}C
[6]	^{132}Sn *
[26]	^{14}N *, ^{16}O, ^{20}Ne *, ^{24}Mg, ^{27}Al, ^{28}Si *, ^{32}S, ^{40}Ar, ^{40}Ca, ^{56}Fe, ^{58}Ni *
[29]	^{208}Pb *
[30]	^{238}U
[31]	^{124}Xe, ^{136}Xe
[32]	^{136}Xe
[33,34]	^{92}Mo *

Figure 7 shows the best f_{EE} versus mass number, for both our experimental data (red dots) and the data from literature (orange squares and blue bold crosses). Nuclei which have a smaller separation energy for protons than for neutrons, which

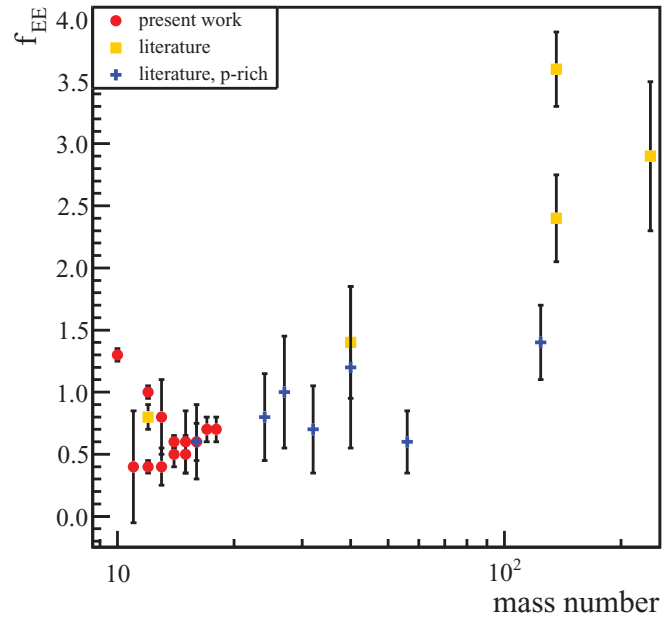

FIG. 7. Optimal excitation energy multiplication factor vs the mass number. Error bars indicate the estimated uncertainty, see text for details on the calculation. (Red) dots represent the present data, while (orange) squares indicate data from Refs. [6,26,29–32], and (blue) bold crosses represent data from Refs. [26,31,33,34] for isotopes that have a larger neutron separation energy than proton separation energy. A clear difference between lighter and heavier nuclei is visible.

causes the particle evaporation after the reaction to be different, are marked differently (blue bold crosses). The figure shows that the excitation energy multiplication factor increases with increasing mass.

Tarasov *et al.* [35] found, for fragmentation of ^{82}Se at 139A MeV, an excitation energy of 15 MeV per abraded nucleon with a different version of the abrasion-ablation model. Even though central collisions are also included, this is consistent with our findings. Unfortunately the region between masses 60 and 130 does not contain any data, so the transition from light to heavy masses is not very conclusive.

Please note that the selection of the reaction channels (restriction to $1pxn$ with $0 \leqslant x \leqslant 5$) included in our optimization of the f_{EE}, selects only peripheral reactions. This physics selection influences the result of the best fit f_{EE}, thus the results presented here are not in conflict with previous $f_{\mathrm{EE}} = 2$ results including the complete set of daughter nuclei.

One can also observe that factors other than the mass influence the induced average excitation energy, due to the large spread of the optimal f_{EE} values. Concerning light nuclei, the description of the prefragment excitation energy in ABRABLA07 would benefit from improvement, since for these nuclei the influence of the nuclear structure and single-particle energies plays a bigger role. See, e.g., Ref. [36] for the importance of nuclear structure on prefragment excitation energy. Performing a simple test, decreasing the default potential depth in ABRABLA07 [7] from 47.4 to 40 MeV, we find no significant influence of that parameter on the ability of ABRABLA07 to reproduce our experimental data.

VII. CONCLUSIONS

We have systematically measured $1pxn$ removal cross sections for 14 neutron-rich carbon and boron isotopes in one single experiment. These new data are used for comparison with model calculations. The EPAX model deviates significantly from the experimental data. The comparison of ABRABLA07 with the new data yields the necessity for a smaller average excitation energy in the model calculations for these nuclei. With that, the calculation reproduces the data surprisingly well, even though there are some deviations. Including additional data from literature we find that the average excitation energy in ABRABLA07 for best reproduction of experimental data on $1pxn$ ($0 \leqslant x \leqslant 5$) reactions increases with increasing mass. This should be taken into account for future calculations of light nuclei with this model.

However, the comparison to data also demonstrates that changing the average excitation energy per abraded nucleon alone is insufficient for a full description of the experimental data. The behavior of the induced excitation energy is complex, and more investigations are needed. A potential influence of the impact parameter on the f_{EE}, which is indicated by our results for heavy nuclei differing from the adopted value of $f_{\mathrm{EE}} = 2$, would be interesting to investigate further. A more realistic estimate of prefragment excitation energy would probably improve the model not only with regard to light isotopes, but also more generally.

Due to the model's extreme relevance in helping us understand the isotope fragmentation production mechanism, we feel that additional theoretical improvements of the relatively successful abrasion-ablation model are necessary. In particular a better understanding and prediction of the average excitation energy per abraded nucleon would be beneficial.

ACKNOWLEDGMENTS

We thank the FRS and the GSI accelerator staff for their efforts. We thank Alexandra Kélic-Heil for providing us with the ABRABLA07 code and for fruitful discussions. This work was supported by the Swedish Research Council. O.T. was supported by the Spanish Research Council under project FPA2012-32443, C.A.B. acknowledges support from the U.S. DOE Grant No. DE-FG02-08ER41533 and the U.S. NSF Grant No. 1415656. L.M.F. acknowledges support by the Spanish Research Council under project FPA2013-41267-P and M.R. was supported by GSI (F&E, DR-ZUBE), German BMBF (06DR134I and 05P09CRFN5), the Nuclear Astrophysics Virtual Institute (NAVI, HGF VH-VI-417) and the Helmholtz Association Detector Technology and Systems Platform. T.K. acknowledges support by the German BMBF No. 06DA9040I, No. 05P12RDFN8, and No. 05P15RDFN1. C.W. acknowledges funding by the UK STFC No. ST/E500651/1, while N.A. and M.F. acknowledge funding by the UK STFC No. ST/F011989/1.

[1] K. Riisager, Phys. Scr. **T152**, 014001 (2013).
[2] R. Kanungo, Phys. Scr. **T152**, 014002 (2013).
[3] I. Tanihata, H. Hamagaki, O. Hashimoto, Y. Shida, N. Yoshikawa, K. Sugimoto, O. Yamakawa, T. Kobayashi, and N. Takahashi, Phys. Rev. Lett. **55**, 2676 (1985).
[4] K. Sümmerer, Phys. Rev. C **86**, 014601 (2012).
[5] T. Nilsson, Nucl. Instrum. Methods B **317**, 194 (2013).
[6] D. Pérez-Loureiro *et al.*, Phys. Lett. B **703**, 552 (2011).
[7] J.-J. Gaimard and K.-H. Schmidt, Nucl. Phys. A **531**, 709 (1991).
[8] K. Sümmerer and H. Weick (C translation), " [C source code] EPAX Version 3 : An Empirical Parametrization of Projectile-Fragmentation Cross Sections, Klaus Suemmerer, 17.01.2013", 2013, https://www-alt.gsi.de/documents/DOC-2012-May-55.html.
[9] A. Leistenschneider, T. Aumann, K. Boretzky, L. F. Canto, B. V. Carlson, D. Cortina, U. Datta Pramanik, Th. W. Elze, H. Emling, H. Geissel, A. Grünschloss, K. Helariutta, M. Hellström, M. S. Hussein, S. Ilievski, K. L. Jones, J. V. Kratz, R. Kulessa, Le Hong Khiem, E. Lubkiewicz, G. Münzenberg, R. Palit, P. Reiter, C. Scheidenberger, K.-H. Schmidt, H. Simon, K. Sümmerer, E. Wajda, and W. Walús, Phys. Rev. C **65**, 064607 (2002).
[10] H. Geissel, P. Armbruster, K. H. Behr, A. Brünle, K. Burkard, M. Chen, H. Folger, B. Franczak, H. Keller, O. Klepper, B. Langenbeck, F. Nickel, E. Pfeng, M. Pfützner, E. Roeckl, K. Rykaczewski, I. Schall, D. Schardt, C. Scheidenberger, K.-H. Schmidt, A. Schröter, T. Schwab, K. Sümmerer, M. Weber, G. Münzenberg, T. Brohm, H.-G. Clerc, M. Fauerbach, J.-J. Gaimard, A. Grewe, E. Hanelt, B. Knödler, M. Steiner, B. Voss, J. Weckenmann, C. Ziegler, A. Magel, H. Wollnik, J. P. Dufour,

Y. Fujita, D. J. Vieira, and B. Sherrill, Nucl. Instrum. Methods B **70**, 286 (1992).
[11] V. Metag, R. D. Fischer, W. Kühn, R. Mühlhans, R. Novotny, D. Habs, U. v. Helmholt, H. W. Heyng, R. Kroth, D. Pelte, D. Schwalm, W. Hennerici, H. J. Hennrich, G. Himmerle, E. Jaeschke, R. Repnow, W. Wahl, E. Adelberger, A. Lazzarini, R. S. Simon, R. Albrecht, and B. Kolb, Nucl. Phys. A **409**, 331 (1983).
[12] F. Wamers, Ph.D. thesis, TU Darmstadt, 2011.
[13] K. Mahata, H. T. Johansson, S. Paschalis, H. Simon, and T. Aumann, Nucl. Instrum. Methods A **608**, 331 (2009).
[14] T. Blaich *et al.* (LAND Collaboration), Nucl. Instrum. Methods A **314**, 136 (1992).
[15] R. Plag, Documentation on the LAND/R^{3}B tracker, GSI 2015, http://ralfplag.de/tracker.
[16] T. Ogawa, T. Sato, S. Hashimoto, D. Satoh, S. Tsuda, and K. Niita, Phys. Rev. C **92**, 024614 (2015).
[17] K. Helariutta, J. Benlliure, M. V. Ricciardi, and K.-H. Schmidt, Eur. Phys. J. A **17**, 181 (2003).
[18] P. J. Karol, Phys. Rev. C **11**, 1203 (1975).
[19] K.-H. Schmidt, T. Brohm, H.-G. Clerc, M. Dornik, M. Fauerbach, H. Geissel, A. Grewe, E. Hanelt, A. Junghans, A. Magel, W. Morawek, G. Münzenberg, F. Nickel, M. Pfützner, C. Scheidenberger, K. Sümmerer, D. Vieira, B. Voss, and C. Ziegler, Phys. Lett. B **300**, 313 (1993).
[20] A. Kelic, M. V. Ricciardi, and K.-H. Schmidt, in *Joint ICTP-IAEA Advanced Workshop on Model Codes for Spallation Reactions Trieste, Italy, February 4–8, 2008* (IAEA, Vienna, Austria, 2009).
[21] V. F. Weisskopf and D. H. Ewing, Phys. Rev. **57**, 472 (1940).
[22] A. Gilbert and A. G. W. Cameron, Can. J. Phys. **43**, 1446 (1965).
[23] A. V. Ignatyuk, in *Proceedings on of the Conference Bologna 2000: Structure of the Nucleus at the Dawn of the Century, Bologna, Italy 29 May–3 June 2000*, edited by G. C. Bonsignori, M. Bruno, A. Ventura, and D. Vretenar (World Scientific, Singapore, 2001).
[24] G. Audi, M. Wang, A. H. Wapstra, F. G. Kondev, M. MacCormick, X. Xu, and B. Pfeiffer, Chin. Phys. C **36**, 1287 (2012).
[25] M. Wang, G. Audi, A. H. Wapstra, F. G. Kondev, M. MacCormick, X. Xu, and B. Pfeiffer, Chin. Phys. C **36**, 1603 (2012).
[26] W. R. Webber, J. C. Kish, and D. A. Schrier, Phys. Rev. C **41**, 547 (1990).
[27] J. M. Kidd, P. J. Lindstrom, H. J. Crawford, and G. Woods, Phys. Rev. C **37**, 2613 (1988).
[28] K. Sümmerer, Phys. Rev. C **87**, 039903(E) (2013).
[29] T. Kurtukian-Nieto, J. Benlliure, K.-H. Schmidt, L. Audouin, F. Becker, B. Blank, E. Casarejos, F. Farget, M. Fernández Ordóñez, J. Giovinazzo, D. Henzlova, B. Jurado, J. Pereira, and O. Yordanov, Phys. Rev. C **89**, 024616 (2014).
[30] A. R. Junghans, M. de Jong, H.-G. Clerc, A. V. Ignatyuk, G. A. Kudyaev, and K.-H. Schmidt, Nucl. Phys. A **629**, 635 (1998).
[31] D. Henzlova, K.-H. Schmidt, M. V. Ricciardi, A. Kelić, V. Henzl, P. Napolitani, L. Audouin, J. Benlliure, A. Boudard, E. Casarejos, J. E. Ducret, T. Enqvist, A. Heinz, A. Junghans, B. Jurado, A. Krása, T. Kurtukian, S. Leray, M. F. Ordóñez, J. Pereira, R. Pleskač, F. Rejmund, C. Schmitt, C. Stéphan, L. Tassan-Got, C. Villagrasa, C. Volant, A. Wagner, and O. Yordanov, Phys. Rev. C **78**, 044616 (2008).
[32] J. Benlliure, M. Fernández-Ordóñez, L. Audouin, A. Boudard, E. Casarejos, J. E. Ducret, T. Enqvist, A. Heinz, D. Henzlova, V. Henzl, A. Kelic, S. Leray, P. Napolitani, J. Pereira, F. Rejmund, M. V. Ricciardi, K.-H. Schmidt, C. Schmitt, C. Stéphan, L. Tassan-Got, C. Volant, C. Villagrasa, and O. Yordanov, Phys. Rev. C **78**, 054605 (2008).
[33] B. Fernández-Domínguez, R. C. Lemmon, B. Blank, M. Chartier, D. Cortina-Gil, J. L. Durell, H. Geissel, J. Gerl, S. Mandal, F. Rejmund, and K. Sümmerer, Eur. Phys. J. **A25**, 193 (2005).
[34] B. Fernández-Domínguez, R. C. Lemmon, B. Blank, M. Chartier, D. Cortina-Gil, J. L. Durell, H. Geissel, J. Gerl, S. Mandal, F. Rejmund, and K. Sümmerer, Eur. Phys. J. **A25**, 473 (2005).
[35] O. B. Tarasov, M. Portillo, D. J. Morrissey, A. M. Amthor, L. Bandura, T. Baumann, D. Bazin, J. S. Berryman, B. A. Brown, G. Chubarian, N. Fukuda, A. Gade, T. N. Ginter, M. Hausmann, N. Inabe, T. Kubo, J. Pereira, B. M. Sherrill, A. Stolz, C. Sumithrarachichi, M. Thoennessen, and D. Weisshaar, Phys. Rev. C **87**, 054612 (2013).
[36] J. Benlliure, EPJ Web Conf. **88**, 00028 (2015).